Radio Science, Volume ???, Number , Pages 1–27,

Direct MSTID mitigation in precise GPS processing

Manuel Hernández-Pajares[1], Pawel Wielgosz[2], Jacek Paziewski[2], Anna Krypiak-Gregorczyk[2], Marta Krukowska[2], Katarzyna Stepniak[2], Jan Kaplon[3], Tomasz Hadas[3], Krzysztof Sosnica[3], Jaroslaw Bosy[3], Raul Orus-Perez[4], Enric Monte-Moreno[1], Heng Yang[1], Alberto Garcia-Rigo[1] and Germán Olivares-Pulido[1]

[1]Universitat Politècnica de Catalunya, Barcelona, Spain (manuel@ma4.upc.edu)

[2]University of Warmia and Mazury in Olsztyn, Olsztyn, Poland (p.a.wielgosz@gmail.com)

[3]WUELS, Wroclaw, Poland (jaroslaw.bosy@igig.up.wroc.pl)

[4]ESA-ESTEC, Noordwijk, The Netherlands (raul.orus.perez@esa.int)

In this paper, the authors summarize one simple and efficient approach developed to mitigate the problem in precise GNSS positioning caused by the most frequent ionospheric wave signatures: the Medium Scale Travelling Ionospheric Disturbances (MSTIDs). The direct GNSS Ionospheric Interferometry technique (hereinafter dGII), presented in this paper, is applied for correcting MSTID effects on precise Real Time Kinematic (RTK) and tropospheric determination. It consists on the evolution of the former climatic Differential Delay Mitigation Model for MSTIDs (DMTID), for real-time conditions, using ionospheric data from a single permanent receiver only. The performance is demonstrated with networks of GNSS receivers in Poland, treated as users under real-time conditions, during two representative days in winter and summer seasons (days 353 and 168 of year 2013). In range domain, dGII typically reduces the ionospheric delay error up to 10-90%. The main dGII impact on precise positioning is that we can obtain reliable RTK position faster. In particular the ASR (ambiguity success rate) parameter increases , from 74% to 83%, with respect to the original uncorrected observations. The average of time to first fix is shortened from 30s to 13s.. The improvement in troposphere domain was most difficult to demonstrate.

1. Introduction

The Medium Scale Travelling Ionospheric Disturbances (MSTIDs) are the ionospheric signatures of waves, which are the ones most frequently affecting the precise Global Navigation Satellite Systems (GNSS) processing (see for instance Hernández-Pajares et al. 2006). The MSTIDs present up to few TECUs of amplitude in solar cycle maximum conditions (1 Total Electron Content Unit = 1 TECU = $10^{16}\mathrm{m}^{-2} \simeq 16cm$ delay in L1 signal) with typical periods from several minutes to less than one hour, and velocities from 50 to 300 m/s, typically equatorward during daytime in fall and winter seasons, and westward during night in spring and summer seasons (see for instance Hernández-Pajares et al. 2012).

The MSTID modelling has become feasible thanks to the availability of dual-frequency GNSS, like the Global Positioning System (GPS), which has become likely the main ionospheric sounder in terms of both temporal and spatial resolution and precision (Shagimuratov et al. 2002, Hernández-Pajares et al. 2011, Krypiak-Gregorczyk et al. 2013). Indeed, GNSS is able to provide clear views of the same MSTID amplitude and propagation, either in receivers placed up to few tens of kilometers in local networks (see Figure 1), or from extense dense networks of hundreds of receivers, such as those in Japan or California (see Figure 2), corresponding to the same region and time interval as in the previous figure.

Although different techniques and applications are affected by MSTIDs (like precise GNSS positioning and Very Large Base Interferometry, VLBI), it would be too difficult to determine in real time the exact cause behind each individual instances of TIDs, and several potential sources are contemplated by different authors (see Table 1 in Hernández-Pajares et al. 2012 for additional details and references), such as, in decreasing order of feasibility or potential influence:

1. The Solar Terminator.

2. The Perkins instability (in order to explain the preferred westward propagation of local winter MSTIDs at night).

3. Particle precipitation at the auroral zone, which seems associated to the -sporadic- Large Scale TIDs (LSTIDs), with wavelengths around 1000 km and velocities within the range of 400- 1000 m/s.

4. Meteorological activity.

New or evolved physical and data-driven models have been proposed recently to reproduce MSTID features: the simultaneous occurrence of nighttime MSTIDs at the magnetic conjugate stations, in Yokoyama (2014); or in Deng et al. (2013), where the detrended Total Electron Content (TEC) from the German national network is interpolated to try to show up MSTID wave fronts, and then compared with the corresponding planar wave model in some given events. In another recent work (Penney and Jackson-Booth 2015) the authors detrend the Slant Total Electron Content (STEC) and correct the ionospheric pierce point movement, in a novel way.

Although the MSTID amplitude in not very important in relative terms, compared with the typical background electron content, MSTID's ondulatory nature makes them likely the main non-linear error affecting precise GNSS processing, for instance in RTK or Wide Area Real Time Kinematic (WARTK) techniques (see Wielgosz et. 2005, Hernandez-Pajares et al. 2006), or in Coster and Tsugawa (2015) and in Paziewski (2016). Regarding their mitigation a new approach has been recently proposed by Sieradzki & Paziewski 2016. By means of the observed TEC rate, the user is able to estimate a single initial double-differenced STEC per phase continuous arch.

Moreover, in the last few years, an increase of research in additional aspects of the Medium Scale Travelling Ionospheric Disturbances can be appreciated as well:

- Estimating its 3D structure by means of the Computerized Tomography applied to wide very dense GNSS ground networks like GEONET (Ssessanga et al. 2015, Chen et al. 2016).
- Signatures of natural and artificial events like major earthquakes and nuclear explosions (Jin et al. 2014, Zhang & Tang 2015),
- Recent works formed on the potential mechanisms to form the MSTIDS are Jonah et al. (2016) where the strong troposphere convection as seed mechanism of the Atmospheric Gravity Waves to trigger MSTTDS, is illustrated with collocated turbulence, temperature and electron content data.
- Observations of MSTIDS with different techniques beyond GPS: LOFAR (Mevius et al. 2016), OI 630.0nm all-sky image (Stefanello et al. 2015) and AM radio transmissions (confirmed by simultaneous GPS total electron content, Digisonde, and Super Dual-Auroral Radar Network coherent backscatter radar measurements, Chilcote et al. 2015).

However the MSTID determination and application to precise GNSS positioning typically faces the lack of enough populated local GNSS networks over many regions, in order to apply the state of the art MSTID propagation techniques. Is in this context where the *direct GNSS Ionospheric Interferometry* (dGII) is introduced and applied as a simple way of mitigating the MSTID effect on GNSS positioning.

The layout of the manuscript is the following: After this introduction, the pros and cons of the main existing MSTID modelling techniques are described in section 2. In section 3, dGII is introduced and illustrated by means of a case study. The two experiments in winter and summer time conditions will be described in section 4, including the dGII assessments in terms of MSTID mitigation in range, precise positioning and tropospheric domains Finally, section 5. summarizes the conclusions.

2. Main existing MSTID modelling techniques

We can divide the main approaches to characterize the propagation of MSTIDs with GNSS within two families:

1. The GNSS Massive Ionospheric Detrending (GMID) method: the propagation of the MSTIDs (or any ionospheric perturbation with power in the spectral domain retained after the detrending, typically between 300s and 3000s) can be directly seen from the detrended VTEC, when, first, the separations between ground receivers is less than half wavelength (also referred to as semi-wavelength); and, second, when, moreover, such close permanent receivers are distributed over regions of hundreds of kilometers of extension (at least two wavelengths, see for instance Tsugawa et al.

2007b), in order to properly identify the wavefronts. One advantage of this approach is that it is not restricted to the most frequent case of ionospheric waves (a single train of planar waves) as it can be seen in Figure 3 and in Liu et al. 2011, for co-seismic circular ionospheric waves.

The great practical disadvantage is that such local and extended GNSS networks are available on just few sites, where they were mainly deployed for seismicity monitoring (such as GEONET network in Japan, or Sourth California GNSS Integrated Network, SCIGN, in USA, see Figure 4). One of the first applications of the GMID approach, including data of such networks, can be found in Tsugawa et al. 2007a-b. One example for SCIGN has been previously introduced (see Figure 2, from Hernández-Pajares et al. 2012).

2. The GNSS Ionospheric Interferometric (GII) techniques derive the MSTID propagation velocity from the difference of MSTID phase and associated phase delay among reference receivers. It is computed from the detrended and bandwidth filtered (Fourier transform) VTEC, obtained from the ionospheric (geometry-free) combination of dual-frequency GNSS data. The MSTID time delay is computed basically in two different ways, for each given GNSS satellite in view from a GNSS ground network, with a diameter less than the half of the typical MSTID wavelength (e.g. ¡ 50 km):

(i) By direct correlation of the detrended and bandwidth filtered VTEC, corresponding to each given satellite observed from a given receiver, regarding to the reference receiver (Hernández-Pajares et al. 2006b, Husin et al. 2011).

(ii) By substracting the complex phase for the reference receiver from the corresponding complex phase of the dominant mode (after the Fourier transform) for the given receiver (Hernández-Pajares et al. 2012).

One important advantage of this approach is that just few tens of GNSS receivers within local networks with a diameter of less than half of the wavelength, i.e. less than few tens of kilometers, are enough to give support to large regions of many hundreds of kilometers, due to the large extent of the MSTID planar wave behavior (Tsugawa et al. 2007b). Therefore:

- There are more GNSS facilities already suitable for GII in different regions of the world, compared with GMID (like available networks in Venice, New Zealand, California, Alaska or Hawaii, see Hernández-Pajares et al. 2012).

- The deployment of Local Networks is in any case much cheaper than the deployment of extense dense networks, like GEONET or SCIGN.

However GII presents some significant drawbacks:

- Such local networks are not easily available worldwide, like in most part of Europe, including Poland and other Central European countries, impeding or difficulting the nowcasting of MSTIDs (one main issue found in this research).

- It is based on the assumption of a single dominant planar wave, and this is not the case during some infrequent events commented above. Indeed, although two or more planar waves in different directions could be considered by extending the analysis to several dominant frequencies in parallel, the circular waves (Figure 3) cannot be properly characterized by GII.

We have taken into account the main goal of this work: to model and mitigate the the effect of the MSTID propagation in estimation for large regions of the world, such as East Europe, where no simultaneously extended and dense enough networks are available. In this context we have taken GII as baseline (see scenario at Figure 5). The main characteristics of the reference GII implementation (hereinafter called "comprehensive" GII, cGII) are summarized in the next section.

3. Comprehensive GNSS Ionospheric Interferometry (cGII)

The initially selected implementation of the MSTID detection and propagation estimation algorithm, cGII, is the evolved version presented in Hernández-Pajares et al. (2012) (regarding previous versions, see Hernández-Pajares et al. 2006b and Husin et al. 2011, where more details can be found). The method is based in the cross-correlation of the detrended Vertical Total Electron Content (VTEC) values observed for a given GPS satellite within a local network (see Hernández-Pajares et al. 2006b), but done directly in the frequency domain. Indeed, the MSTID time delay is obtained from the user-reference receiver subtraction of the complex phase of the dominant Fourier Transform terms, which allows to determine the propagation velocities, with a significant computation offloading (adequate for processing vast amounts of data), while being able to deal with several planar waves at different frequencies and with different velocities. cGII consists on the following steps:

1. Preprocessing, consisting on two phases:

(i) The TEC detrending, performed to make clear the MSTID signatures (for each given GNSS satellite), which can be done at least in two different ways:

a. Double difference in time of the ionospheric (geometry-free) combination of dual-frequency carrier phases, LI=L1-L2, and under the absence of cycle slips, with time separations of 300 s (see Hernández-Pajares et al. 2012).

b. Subtracting STEC from a smooth ionospheric model, exemplified in this work by the UPC GIM "UQRG" computed with tomographic and kriging techniques (see Hernández-Pajares et al 1999, Orús et al. 2004), at spatial and temporal scales of few hundreds of kilometers and 900 seconds (i.e. of the order of the MSTID wavelengths and periods).

(ii) The Fourier transform (in fact the Fast Fourier transform algorithm, FFT), which is applied to the detrended VTEC to show up the main modes, in particular the predominant frequency f (which can vary on time).

2. The MSTID propagation delay, Δt, from the reference to the given permanent receiver is given by the difference of complex phase of the dominant Fourier term in both the user and reference receivers (Φ_f)user-(Φ_f)ref (see again Hernández-Pajares et al. 2012).

3. Finally the MSTID velocity is estimated and provided to the users:

(i) From all the values Δt observed from all the permanent network receivers, the MSTID velocity is computed for each given satellite, taking consistently into account the ionospheric pierce point movement (see above mentioned reference).

(ii) With such MSTID velocity vector (estimated every epoch, i.e. each 30 seconds), the time delay is consistently computed and applied by the user to the GNSS network ionospheric corrections.

Nevertheless the application of the comprehensive GNSS Ionospheric Interferometry approach -cGII- is limited by the small number of GNSS receivers in the available European Local Networks, within diameters up to ∼50 km. This network size (less or about half of typical MSTID wavelength) is suitable for applying unambiguously the GNSS Ionospheric Interferometry for characterizing MSTID. This problem affects in particular to Poland and other Central European countries, as it can be seen in the limited number density of available receivers (Figure 6).

4. Direct GNSS Ionospheric Interferometry (dGII)

The direct GNSS Ionospheric Interferometry (dGII) approach is introduced to solve the limitation of the cGII technique related to the lack of close enough receivers over many countries in Europe. dGII is directly based on real-time conditions, generalizing the climatological DMTID model presented in Hernandez-Pajares et al. 2006, in a simple and optimized way. It can be summarized as follows:

1. The VTEC detrended, δV, showing up the MSTID signatures for each given GNSS satellite s, is computed directly based on single difference in time of consecutive measurements, for the same pair transmitter-receiver, of the geometry-free combination of dual-frequency GNSS carrier phase measurements LI=L1-L2 (similarly to Deng et al. 2013), and with a time interval of dt=60 sec (an optimal compromise

between MSTID signal level and time-space localization): δV = δLI / M, being M the ionospheric mapping function, which relates the slant TEC with the vertical TEC (see for instance Hernández-Pajares et al. 2011). We consider in this problem the typical simplification of a spherical thin layer placed at 450 kilometers height (used for instance in the global VTEC ionospheric maps provided in IONEX format, see Schaer et al. 1998).

2. We assume that, for a given GPS satellite, the MSTID is affecting first to the reference receiver, and, a certain time Δt later, to the user. Then the MSTID time delay Δt can be estimated by cross-correlating δLIref with δLIuser, assuming initially a slidding window, depending on the distance distribution in the network (i.e. from 600 sec, up to 1 hour, being then this period the di-facto minimal initial user cold-start time in dGII approach for real-time applications). Indeed, this can be always done by selecting as reference receiver one in the network located in Polarward / East direction during fall-winter / spring-summer seasons (see typical MSTID velocities occurrences in terms of season and local time in Hernandez-Pajares et al. 2012). And the distance between them can be still longer than the predominant MSTID wavelength when the unfiltered amplitude signatures, varying on time, allow the proper implicit distinction of the MSTID phase ambiguity.

3. Thanks to the static and precisely known position of permanent receivers distributed in Wide Area GPS networks, it has been demonstrated that it is possible to compute very precise STEC values, Sref, in real-time (see for instance Hernández-Pajares et al. 2000). In this point, we have considered a simple proxy of Sref, from the

L1-L2 measurements calibrated with the VTEC GIM (see Hernández-Pajares et al. 2011), by using the likely most accurate GIM presently available: the tomographic-kriging UPC GIM "UQRG" (see Hernández-Pajares et al. 2016). Then the precise slant ionospheric delay, Sref, provided by the permanent reference receiver for each given GNSS transmitter in view, is taken as a proxy of the user value, Suser, in the following simple RTK-like way: Suser(t)= Vref(t-Δt) Muser(t) where Vref(t-Δt) is the corresponding VTEC measured at the reference receiver Δt seconds before and Muser(t) is the mapping function (see first point above) at the user location and observations time. It has been shown that this approach is more accurate than other simple proxies of Suser(t) such as Sref(t-Δt) –see right-hand plot in Figure 11. In other words, we are assuming that the main VTEC change due to the movement of Ionospheric Pierce Point (IPP) and the MSTID propagation time between the reference receiver and the user is basically due to the wave signature.

4.1. Case study

To clarify the problem and the technique performance we have analyzed in depth the result of applying dGII to the following case study: the GPS satellite PRN15, observed during first day of year 2001, from two receivers belonging to SCIGN, p294 (reference) and p532 (user), see Figure 7.

It can be seen in Figure 8 the typical MSTID southward propagation signature on STEC, during a winter day-time, which is compared with the spatially and temporally smoothed STEC provided by the GIM. It is fully in agreement with the expected velocities for such local-time and season. The result of the preprocessing detrending (point 1 of dGII algorithm, see above) can be seen in Figure 9. In particular it can be seen the periodic contribution of the GIM model discretization (see additional details in corresponding caption). This suggested us not using it for detrending, keeping just the derivative of the direct observation as an smoother detrender. In this way any *contamination* associated to the GIM gridding in the spectrum, and corresponding artifact in the results, is avoided. In upper-left plot of Figure 10, we show the directly observed detrended STEC for reference and user receivers, thus making visible again the propagation delay between them, so that the delay can be computed by cross-correlation (with a sliding window of about 15 minutes, see upper-left plot of Figure 10). We have mainly considered two different ways of applying dGII: (i) to use the instantaneous MSTID time delay maximizing the real-time correlation between the user and the reference receiver detrended STEC; and (ii) to use the common predominant MSTID time delay, available in near real-time or post-processing, which maximizes all correlations, available right after all the observations in each given continuous phase arch of each given satellite have been taken, from both user and reference receivers. By applying to the detrended VTEC (VTEC derivative) of the reference receiver, the instantaneous MSTID time delay on the one hand, and on the other hand the common predominant MSTID time delay (150 s in this case, see the upper-left and upper-right plots of Figure 10), we obtain the bottom-left and bottom-right plots of Figure 10.

The typical comparison of performance of the detrended VTEC (taking as proxy the VTEC derivative) measured from the user side, with the original (no time-shifted), instantaneous and common shifted reference site time series, can be seen at the left-hand side of Figure 11. The corresponding comparison for STEC, translated directly from the reference receiver, or from translated VTEC by means of the on-time user ionospheric mapping function, can be seen at the right-hand side of Figure 11. The following features can be observed:

1. The STEC of the reference receiver synchronously applied (directly, without time shift) performs worse, as expected.

2. We observe the necesity of using consistently the user mapping function, in order to get the best results with this direct approach.

3. The reference STEC synchronized with the predominant common dGII MSTID time delay works slightly better (especially at 22-22.8h) than the instantaneous one (which is less smooth), except for very low elevation (likely related with the highly varying pierce point velocity, see Penney and Jackson-Booth 2015).

4. Error reduction of up to 50-85% of the initial error in MSTID peaks: from +1.5 TECU when the simple simultaneous RTK ionospheric correction is applied, reduced to 0.2-0.7 TECU, when the expected MSTID time delay is applied.

Finally the comparison of the real versus the estimated user STEC, which is computed with the reference site STEC under four different treatments as proxy of user STEC (reference site STEC original, common-time shifted, and common and instantaneous-time shifted with the user mapping function), can be seen in Figure 12, confirming the previous findings. In particular the suitability of the reference site VTEC, which is delayed by the constant MSTID time delay, estimated independently for each phase-continous arch receiver-transmitter, is shown and used in combination with the user mapping function (Figure 12, bottom-right hand side).

Finally, in the next section, we summarize an extensive application of dGII on different realistic scenarios over Poland, in particular its main impact on precise positioning and tropospheric determination is discussed.

5. dGII assessment over Poland in winter and summer conditions

The direct GII MSTID mitigation technique has been applied, emulating real-time conditions, to three different networks over Poland at NE and SW regions, and overall northern part of Poland (RTKfinal_SW-large, RTKfinal_NE-large and BERNESE_final, respectively), during fall/winter and spring/summer experiments (days 353 and 168, 2013) in order to assess the RTK and tropospheric results.

5.1. Assessment on Range Errors

In figures 13 and 14 the network with the corresponding available receivers (left-hand columns), as well as the summary of the dGII performance in range domain for each user reference baseline (right-hand columns), is represented. A winter day (353, 2013) corresponds to Figure 13 and a summer day (168, 2013) to Figure 14.

These results confirm the best performance of dGII based on an estimated common MSTID time delay per satellite phase-continuous arch of data, plus the actual user mapping function (compared with the other three approaches shown in Figure 12), with daily reductions up to 10-90% of the initial range error when the syncronous ionospheric correction of the reference site is taken (which can be interpreted as a proxy of the MSTID range error mitigation in a basic RTK-like approach), under a simple technique and without the need of estimating the MSTID velocity. The cases with worse performance only happen a few times during the winter day, with a maximum increase of error of 8%, and coinciding mostly with baselines almost not affected (i.e. mainly perpendicular) by the MSTID propagation.

5.2. Assessment on Precise GNSS Positioning Performance

The performance of the RTK positioning was evaluated with different strategies and corresponding files of observations (see Table 1 and Table 2) and based on processing several test baselines, in both winter and summer time.

There are some examples below of the application of dGII-derived corrections to kinematic processing over 57 and 81 km baselines. Table 3 presents the indicators of the RTK positioning performance on day of year (DOY) 168 of year 2013. It is clearly visible for both processed baselines that the application of the MSTID corrections (ModRNX(Prop.STEC)) causes the improvement in the ambiguity resolution (AR) domain. In particular, there can be seen the increase of the ambiguity succes rate (ASR) and the significant drop in the time to first fix. Indeed the daily performance can be seen in fourth column in Table 3, with comprises an still strongest time to first fix reduction under the MSTID modelling when the period with MSTID activity is considered only (from 22 epochs to 8 epochs, and from 16 to 9 epoch, for both BOR-KONI and GNIE-KONI baselines). Additional details can be seen in Figure 15. The ambiguity resolution success rate (ASR) is defined here as the ratio of epochs with correctly resolved ambiguities to total number of processed epochs.

TTFF is defined as the number of epochs required for obtaining correct ambiguity resolution in a processed session. By using MSTID corrections we can obtain reliable RTK position much faster. For BOR1-KONI baseline the ASR (ambiguity success rate) parameter increased from 63 to 78 % for ModRNX(Prop.STEC) observations in respect to the original uncorrected observations. For the second baseline the same parameter increased by 9 % to a value of 83 %. The value of time to first fix shortened from almost 30 s to 13 s, and from, 18 s to 16 s, for BOR1 and GNIE rover baselines respectively (Table 1). The repeatability of the kinematic coordinates on 168 DOY are on similar levels for both the strategies. The standard deviation of the mean coordinates varies in the range 11-13 mm, 6-9 mm and 25-36 mm, for N, E, U components respectively.

5.3. Assessment on Tropospheric Delay Estimates

The dGII impact in troposphere domain was verified with 24 daily solutions for experimental network: 6 different sets of RINEX files were processed using two baseline defnition strategies (SHORTEST, STAR) in each experimental campaign (summer and winter). These strategies, as well as OBS-MAX and DEFINED are used for baseline definition in Bernese GNSS Software v. 5.2 (Dach et al., 2015). The SHORTEST strategy leads to create the set of shortest baselines in given setup of processed stations. The STAR strategy creates the set of baselines connecting one reference station with all remaining stations.. The results of the RMS of post-fit residuals of unit weight, station coordinate errors, number of ambiguity resolution (in four ambiguity resolution, AR, strategies), error of estimated Zenith Tropospheric Delay (ZTD) and

ZTD residuals with respect to Regional Reference Frame Sub-Commission for Europe (EUREF) GNSS Positioning Network (EPN) final solution, were investigated in detail.

Negligible differences between solutions were found among the RMS of unit weight, station coordinate errors, and estimated ZTD errors. This is because we used 24-hour sessions for troposphere estimation where MSTID effects affecting a few per cent of observations in a session, vanish out due to large amount of the processed data compared to RTK.

The differences were significant for AR results (Figure 16). In SHORTEST baseline definition strategy, the significant improvement was noticed in Quasi Ionosphere-Free method (QIF) for all developed ionosphere models, while for the remaining AR strategies the results, comparing to RedRNX+CodeION, are very similar, except Prop.STEC model in winter campaign. In STAR strategy, that is consistent with the methodology of MSTID model determination, all three developed models increased the percent of resolved ambiguities with respect to the solution without any ionosphere model ModRNX(Truth.STEC) solution was better than RedRNX+CodeION in every AR strategy, and ModRNX(Prop.STEC) was better that RedRNX+CodeION in QIF strategy (very long baselines). Similar results were obtained with Narrow Lane and Wide Lane strategies.

Significant differences were found in estimated ZTD values. The application of developed models resulted in ZTD biased with respect to EPN final solution and with respect to the solution with the Global Ionospheric VTEC Maps provided by the Center for Orbit Determination in Europe (CODE) to the International GNSS Service, IGS (Figure 17). This bias is caused by the reduced number of observations in RINEX files, as well as by inconsistency with the reference solution, that is based on the CODE ionosphere model. The obtained bias showed that the solutions with ionosphere model including MSTID are different than the EPN final solution (the differences were even larger during the periods of expected MSTID maximum activity), however there is no possibility to assess which one is better.

6. Conclusions

We present in this work an MSTID modeling that overcomes shortcomings of the existing methods. The modelling technique that we present is more suitable for sparse GNSS networks. The direct GNSS Ionospheric Interferometry (dGII) is applied in real-time conditions, and depends only on reference ionospheric data from a single permanent receiver. The performance in range domain can reduce the error up to 10-90%, with only a worsening in some cases up to 8%. Subsequent application of MSTID corrections to relative kinematic positioning resulted in reduction of size and variability of between-pair-of-transmitter-and-receivers Double Differenced (DD) ionospheric residuals during MSTID occurrence. In particular, ambiguity success rate was improved, and the number of epochs required to obtain precise position decreased.

Acknowledgment

The data for this paper are available and it can be requested to any of the authors, in particular to Manuel Hernández-Pajares (Manuel.Hernandez@upc.edu), Pawel Wielgosz (pawel.wielgosz@uwm.edu.pl) and Tomasz Hadas (tomasz.hadas@igig.up.wroc.pl). The work reported in this paper has been supported under a contract of the European Space Agency (PIOM-FIPP). The views presented in the paper represent solely the opinion of the authors and should be considered as R and D results not necessarily impacting the present EGNOS and Galileo system design.

7. References

- Beniguel, Y., Angling, M., Banfi, E., Bourga, C., Cueto, M., Fleury, R., Garcia-Rigo, A., Hamel, P., Hartmann, R., Hernandez-Pajares, M., Jakowski, N., Kauristie, K., Orus, R., Prieto-Cerdeira, R., Valette, J.J. & van de Kamp, M. (2012, December). Ionospheric Effects on GNSS Performance. In Satellite Navigation Technologies and European Workshop on GNSS Signals and Signal Processing,(NAVITEC), 2012 6th ESA Workshop on (pp. 1-8). IEEE.
- Chen, C.H., A. Saito, C. H. Lin, M. Yamamoto, S. Suzuki & G. K. Seemala, Medium-scale traveling ionospheric disturbances by three-dimensional ionospheric GPS tomography, Chen et al. Earth Planet Sp (2016) 68:32.
- Chilcote, M., J. LaBelle, F. D. Lind, A. J. Coster, E. S. Miller, I. A. Galkin, & A. T. Weatherwax (2015), Detection of traveling ionospheric disturbances by medium-

frequency Doppler sounding using AM radio transmissions, Radio Sci., 50, 249-263, doi:10.1002/2014RS005617.

- Coster A. & T. Tsugawa, "The Impact of Traveling Ionospheric Disturbances on Global Navigation Satellite System Services", http://www.ursi.org/proceedings/procga08/papers/fgp1.pdf, October 13, 2015.

- Dach, R., Lutz, S., Fridez, P. & Walser P. (Ed) (2015). Bernese GNSS Software Version 5.2. Astronomical Institute, University of Bern, Bern, Switzerland, 142-143.

- Deng, Z., Schön, S., Zhang, H., Bender, M., & Wickert, J. (2013). Medium-scale traveling ionospheric disturbances (MSTID) modeling using a dense German GPS network. Advances in Space Research, 51(6), 1001-1007.

- Hernández-Pajares, M., Roma-Dollase, D., Krankowski, A., Ghoddousi-Fard, R., Yuan, Y., Li, Z., Zhang, H., Shi, C., Feltens, J., Komjathy, A., Vergados, P., Schaer, S.C., García-Rigo, A. & Gómez-Cama, J.M., Comparing performances of seven different global VTEC ionospheric models in the IGS context, http://igs.org/assets/pdf/W2016-PY0507-Hernandez-Pajares.pdf, IGS WS, Sydney, Australia, Feb. 8-12, 2016.

- Hernández-Pajares, M. (2013), Analysis of the ionospheric signatures before, during and after the Fukushima earthquake, IPRESES project, UPC, Sep. 2013.

- Hernández-Pajares, M., Juan, J. M., Sanz J., Aragón-Àngel A. (2012) Propagation of medium scale traveling ionospheric disturbances at different latitudes and solar cycle conditions, Radio Sci., 47, RS0K05, doi:10.1029/2011RS004951.

• Hernández-Pajares, M., Juan, J. M., Sanz, J., Aragón-Àngel, À., García-Rigo, A., Salazar, D., & Escudero, M. (2011). The ionosphere: effects, GPS modeling and the benefits for space geodetic techniques. Journal of Geodesy, 85(12), 887-907.

• Hernández-Pajares, M., Juan, J. M., & Sanz, J. (2006). Real time MSTIDs modelling and application to improve the precise GPS and GALILEO navigation. In ION GNSS meeting, Sep. 2006, Forth Worth, TX, USA.

• Hernández-Pajares, M., Juan, J. M., & Sanz, J. (2006b). Medium-scale traveling ionospheric disturbances affecting GPS measurements: Spatial and temporal analysis. Journal of Geophysical Research: Space Physics (1978-2012), 111(A7).

• Hernández-Pajares, M., Juan, J. M., Sanz, J., & Colombo, O. L. (2000). Application of ionospheric tomography to real-time GPS carrier-phase ambiguities Resolution, at scales of 400-1000 km and with high geomagnetic activity. Geophysical Research Letters, 27(13), 2009-2012.

• Hernández-Pajares, M., Juan, J. M., & Sanz, J. (1999). New approaches in global ionospheric determination using ground GPS data. Journal of Atmospheric and Solar-Terrestrial Physics, 61(16), 1237-1247.

• Husin, A., M. Abdullah, & M. A. Momani (2011), Observation of medium-scale traveling ionospheric disturbances over Peninsular Malaysia based on IPP trajectories, Radio Sci., 46, RS2018, doi:10.1029/2010RS004408.

• Jonah, O. F., E. A. Kherani, & E. R. De Paula (2016), Observation of TEC perturbation associated with mediumscale traveling ionospheric disturbance and possible seeding mechanism of atmospheric gravity wave at a Brazilian sector, J. Geophys. Res. Space Physics, 121, doi:10.1002/2015JA022273.

- Juan, J. M., Sanz J., Aragón-Àngel A. (2012) Propagation of medium scale traveling ionospheric disturbances at different latitudes and solar cycle conditions, Radio Sci., 47, RS0K05, doi:10.1029/2011RS004951.

- Krypiak-Gregorczyk A., Wielgosz P., Gosciewski D., Paziewski J. (2013) Validation of Approximation Techniques for Local Total Electron Content Mapping. Acta Geodynamica et Geomaterialia Vol. 10, No. 3 (171), 275-283 (DOI: 10.13168/AGG.2013.0027).

- Jin, S., R. Jin, & J. H. Li (2014), Pattern and evolution of seismo-ionospheric disturbances following the 2011 Tohoku earthquakes from GPS observations, J. Geophys. Res. Space Physics, 119, 7914-7927, doi:10.1002/2014JA019825.

- Liu, J.-Y., C.-H. Chen, C.-H. Lin, H.-F. Tsai, C.-H. Chen, & M. Kamogawa (2011), Ionospheric disturbances triggered by the 11 March 2011 M9.0 Tohoku earthquake, J. Geophys. Res., 116, A06319, doi:10.1029/2011JA016761.

- Mevius, M., et al. (2016), Probing ionospheric structures using the LOFAR radio telescope, Radio Sci., 51, 927-941, doi:10.1002/2016RS006028.

- Orús, R., Hernández-Pajares, M., Juan, J. M., & Sanz, J. (2005). Improvement of global ionospheric VTEC maps by using kriging interpolation technique. Journal of Atmospheric and Solar-Terrestrial Physics, 67(16), 1598-1609.

• Paziewski, J. (2016). Study on desirable ionospheric corrections accuracy for network-RTK positioning and its impact on time-to-fix and probability of successful single-epoch ambiguity resolution. Advances in Space Research, 57(4), 1098-1111.

• Penney, R. W., & N. K. Jackson-Booth (2015), Mitigating satellite motion in GPS monitoring of traveling ionospheric disturbances, Radio Sci., 50, 1150-1164, doi:10.1002/2015RS005767.

• Schaer, S., Gurtner, W., & Feltens, J. (1998, February). IONEX: The ionosphere map exchange format version 1. In Proceedings of the IGS AC workshop, Darmstadt, Germany (Vol. 9, No. 11).

• Shagimuratov, I.I., Baran, L.W., Wielgosz, P., & Yakimova, G.A., (2002), The structure of mid- and high-latitude ionosphere during September 1999 storm event obtained from GPS observations, Annales Geophysicae, Vol. 20, No 5, pp. 665-660.

• Sieradzki, R., & Paziewski, J. (2016). MSTIDs impact on GNSS observations and its mitigation in rapid static positioning at medium baselines. Annals of Geophysics, 58(6), A0661.

• Ssessanga, N., Y. H. Kim, & E. Kim (2015), Vertical structure of medium-scale traveling ionospheric disturbances, Geophys. Res. Lett., 42, 9156-9165, doi:10.1002/2015GL066093.

• Stefanello, M.B., Muella, M.T.A.H, Amorim, D.C.M., Machado, C.S., Bageston, J.V., Pimenta, A.A., Martinis, C., Sullivan, C., Bittencourt, J.A., & Schuch, N.J., OI 630.0nm all-sky image Observations of medium-scale traveling ionospheric

Disturbances at geomagnetic conjugate Points , Journal of Atmospheric and Solar-Terrestrial Physics, http://dx.doi.org/10.1016/j.jastp.2015.03.012

- Tsugawa, T., Kotake, N., Otsuka, Y., & Saito, A. (2007a). Medium-scale traveling ionospheric disturbances observed by GPS receiver network in Japan: A short review. GPS Solutions, 11(2), 139-144.

- Tsugawa, T., Otsuka, Y., Coster, A. J., & Saito, A. (2007b). Medium-scale traveling ionospheric disturbances detected with dense and wide TEC maps over North America. Geophysical Research Letters, 34(22).

- Wielgosz, P., Kashani, I., & Grejner-Brzezinska, D.A., (2005), Analysis of Long-Range Network RTK during Severe Ionospheric Storm, Journal of Geodesy, Vol. 79, No. 9, pp. 524-531.

- Yokoyama, T. (2014). Hemisphere-coupled modeling of nighttime medium-scale traveling ionospheric disturbances. Advances in Space Research, 54(3), 481-488.

- Zhang, X. & Tang, L. (2015). Traveling ionospheric disturbances triggered by the 2009 North Korean underground nuclear explosion, Ann. Geophys., 33, 137-142, doi:10.5194/angeo-33-137-2015.

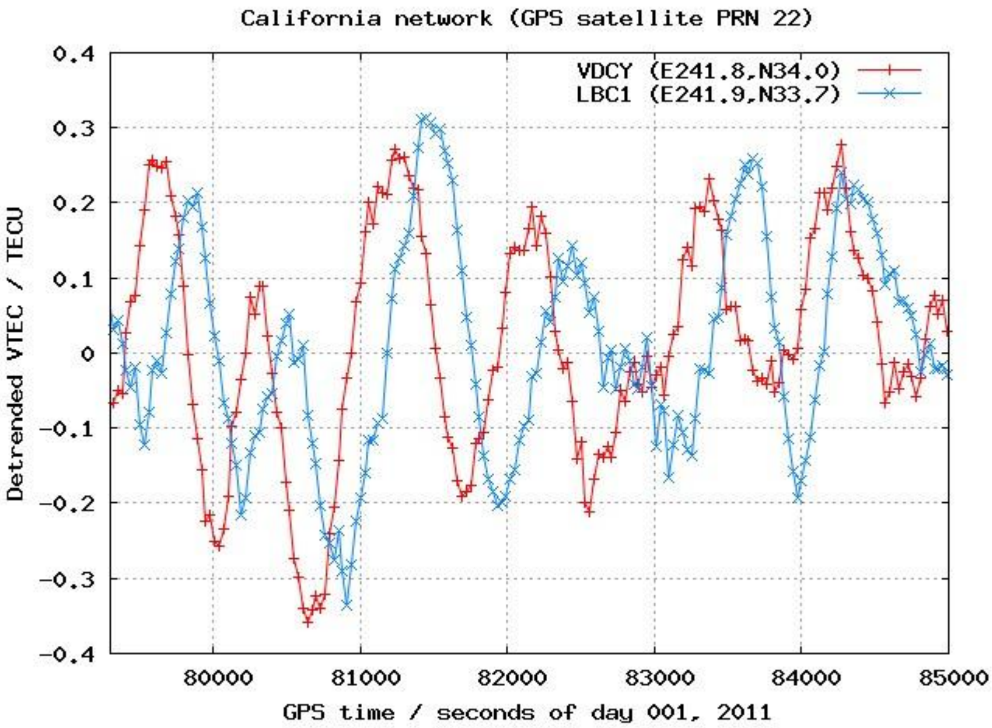

Figure 1. Example of MSTID signature in the detrended Vertical Electron Content (VTEC), directly obtained from the ionospheric combination of GPS carrier phases (see section 3) corresponding to an MSTID affecting GPS satellite PRN 22, advancing from receiver VDCY (E241.8,N34.0) toward LBC1 (E241.9,N33.7) in California network, January 1st, 2011 (reproduced from Hernández-Pajares et al. 2012).

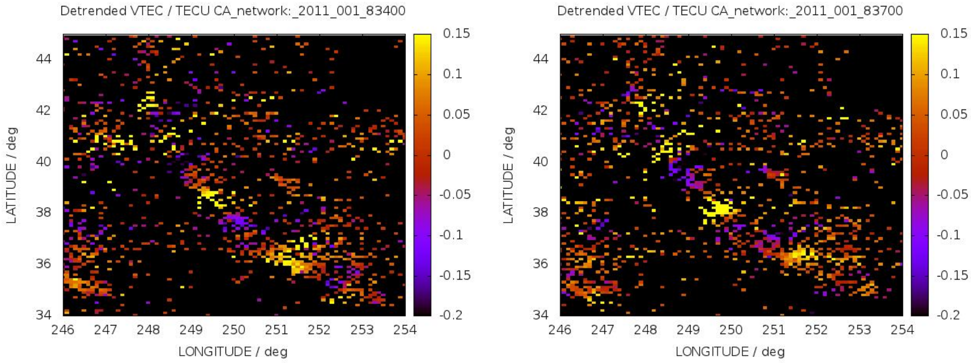

Figure 2. Daytime winter MSTID propagation fronts directly seen from detrended VTEC V (in TECUs; GMID method) over the whole dense network in California and West USA (first day of 2011, for GPS time epochs 83400 and 83700 s, reproduced from Hernández-Pajares et al. 2012).

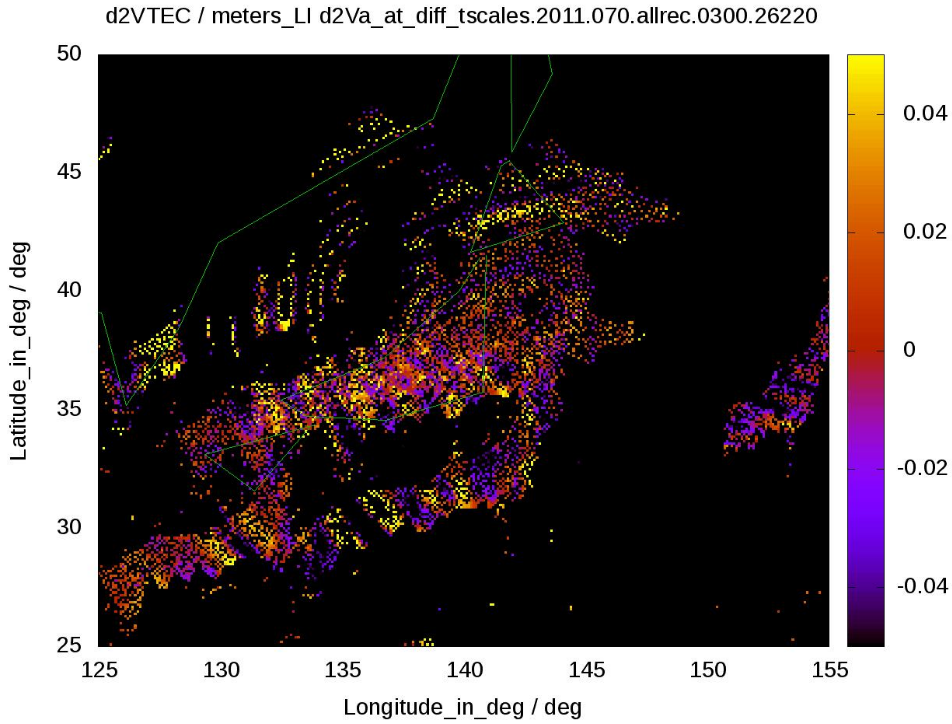

Figure 3. Detrended VTEC obtained from GEONET GPS data, coinciding with the Tohoku earthquake and tsunami (GPS second 26220 of day 70, 2011), where the circular ionospheric waves centered at the earthquake epicenter are evident (extracted from Hernández-Pajares 2013).

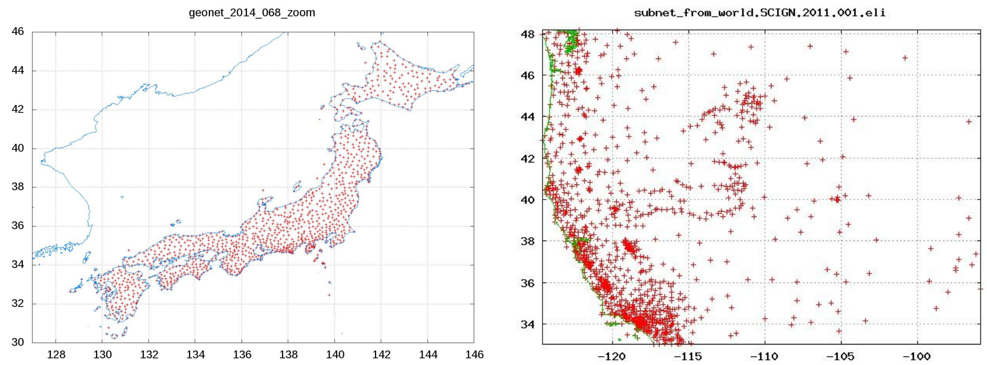

Figure 4. Main part of GEONET GNSS network (left-hand plot, corresponding to deployed receivers during day 68, 2014) and South California Integrated GNSS Network (SCIGN, for day 1, 2011, right-hand plot).

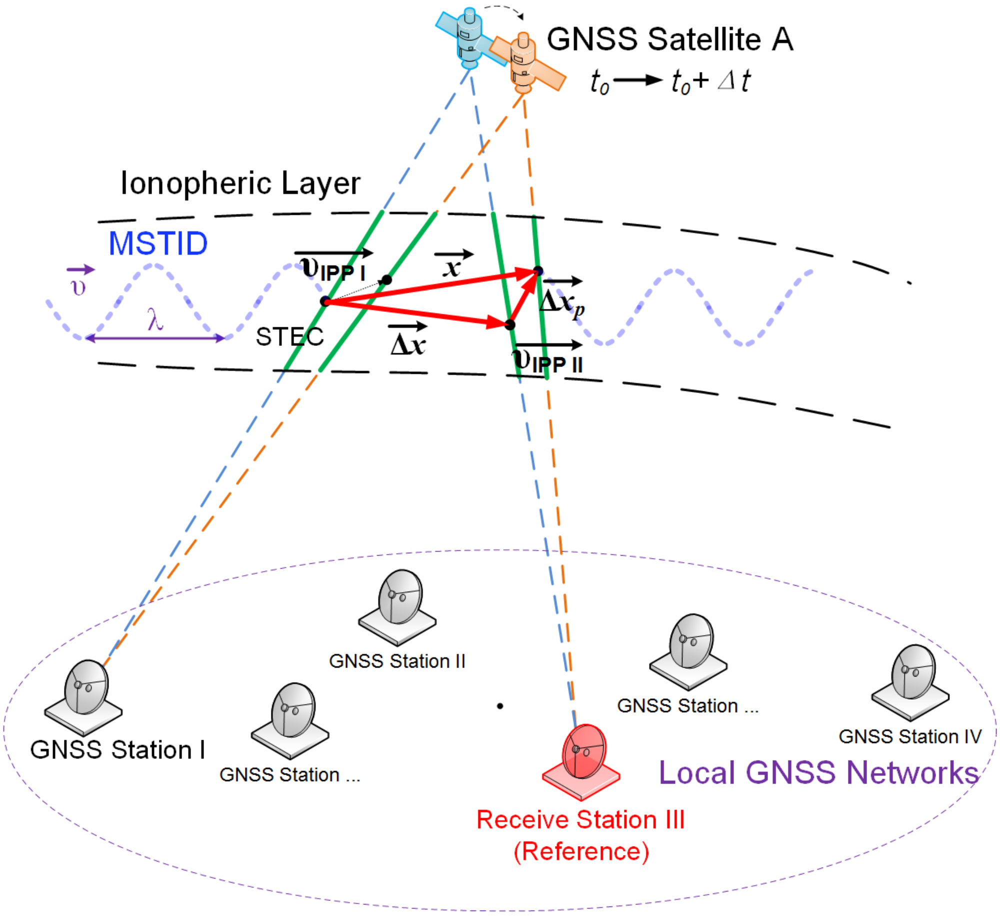

Figure 5. MSTID detection Model from GNSS Networks: The baseline vector between any static receiver and the reference one, Δx, the velocity of the Ionospheric Pierce Point, IPP, and the corresponding movement, Δx_p, during the time Δt, are represented.

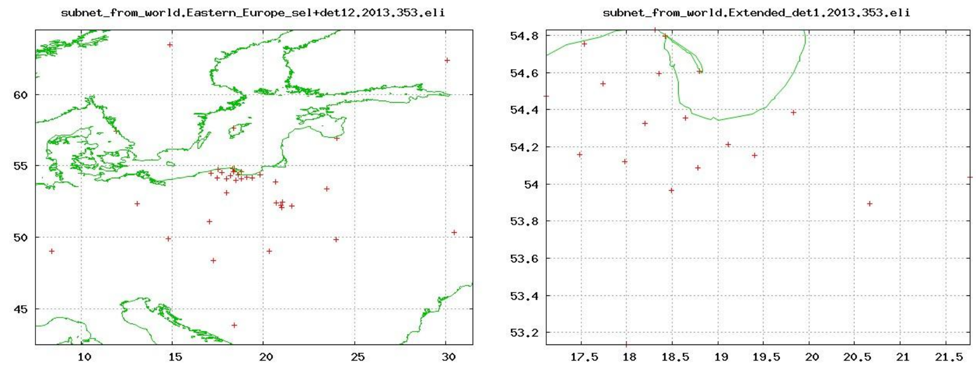

Figure 6. Distribution of GNSS receivers available in Eastern Europe for the study, during day 353, 2013 (left-hand plot, with zoom on the right-hand plot).

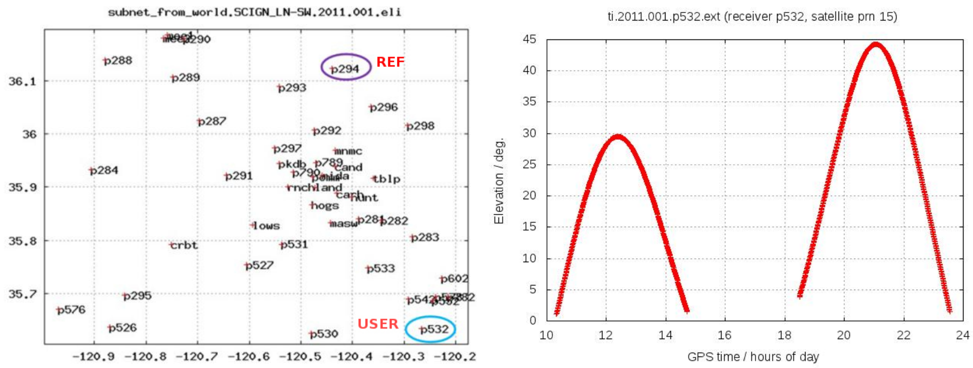

Figure 7. [Left] Location of two GNSS SCIGN receivers (p294 taken as reference -REF- and p532 treated as user -USER-), selected due to its southward-oriented baseline, for the GII test case studies. [Right] The elevation of satellite PRN15 is represented as function of the time from user receiver (PRN15, day 001, 2011).

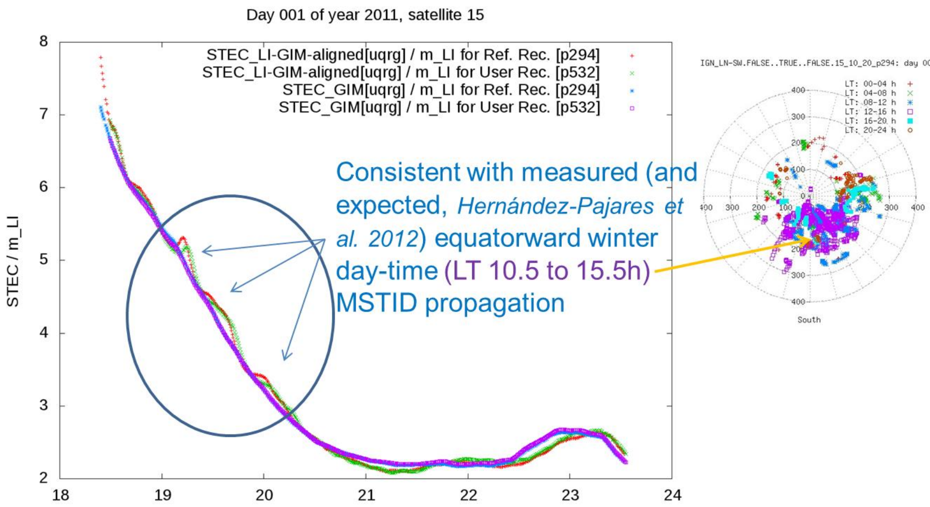

Figure 8. Correspondence of the MSTID signature in calibrated Slant Total Electron Content (STEC) in meters of LI=L1-L2 (left) with the estimated velocity with cGII (right) -SCIGN, day 001, 2011-.

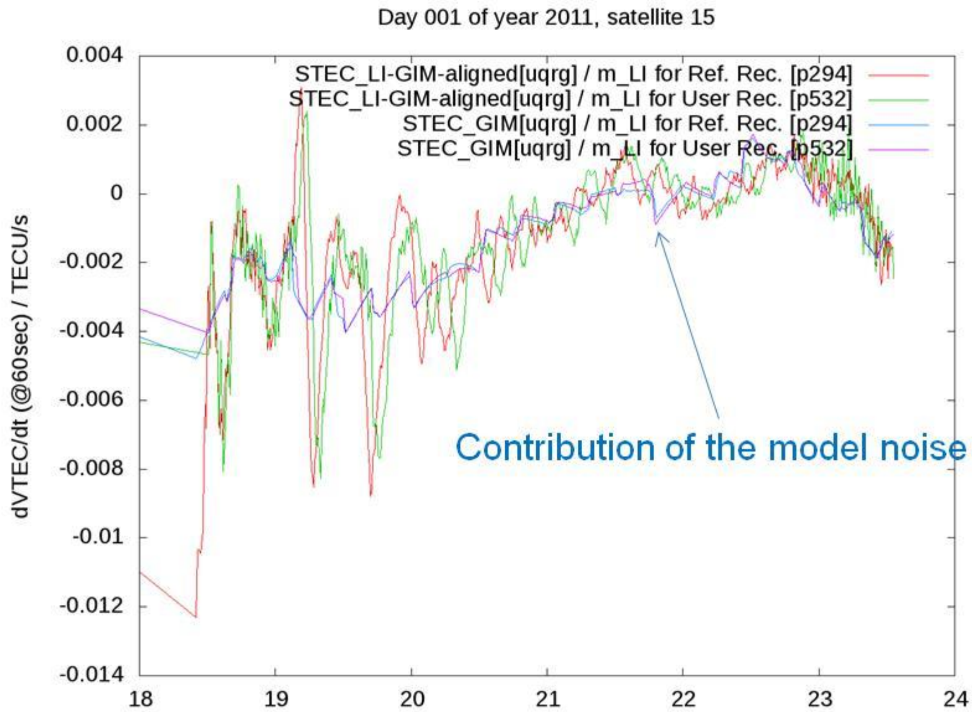

Figure 9. Derivative of the GIM detrended STECs and GIM STECs in dGII case study, projected vertically (dVTEC/dt computed for dt = 60 seconds) where the GIM model noise, with a temporal and spatial resolution too low to capture the MSTID propagation, is evident in the peaks shown in magenta (receivers p294 and p532, satellite PRN15, day 1, 2011).

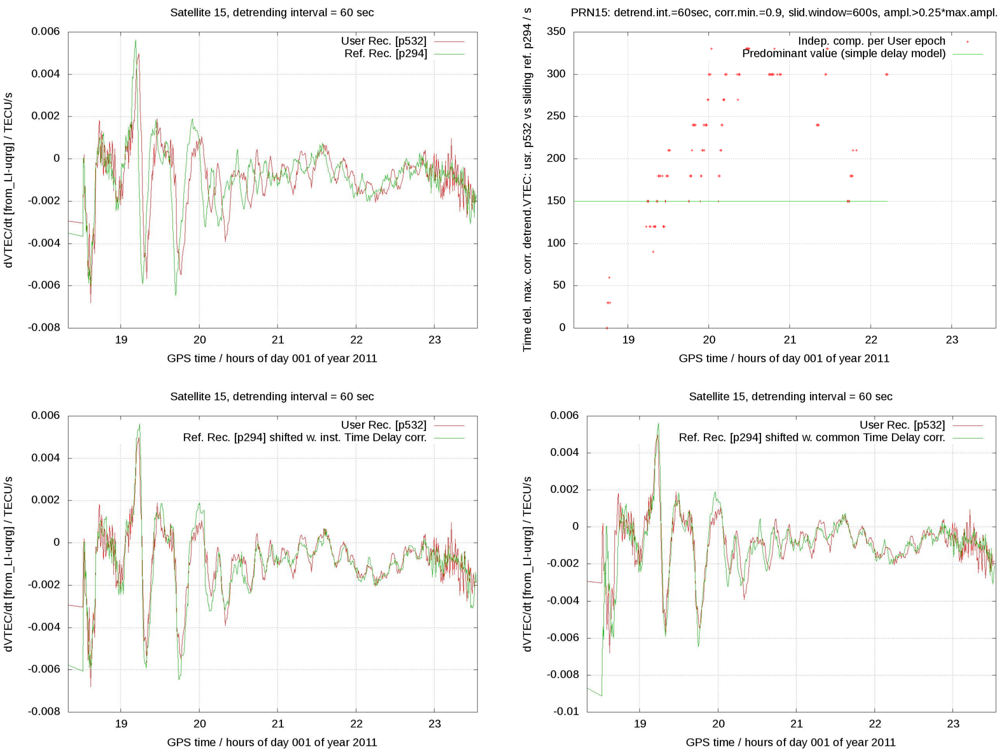

Figure 10. Top-left, bottom-left and bottom-right plots: Plain observed, instantaneously and common dGII-time shifted STEC derivative, respectively, following the estimated MSTID time delay obtained by direct cross correlation (top-right plot) –SCIGN, p294, p532 rec., PRN15, day 001, 2011-.

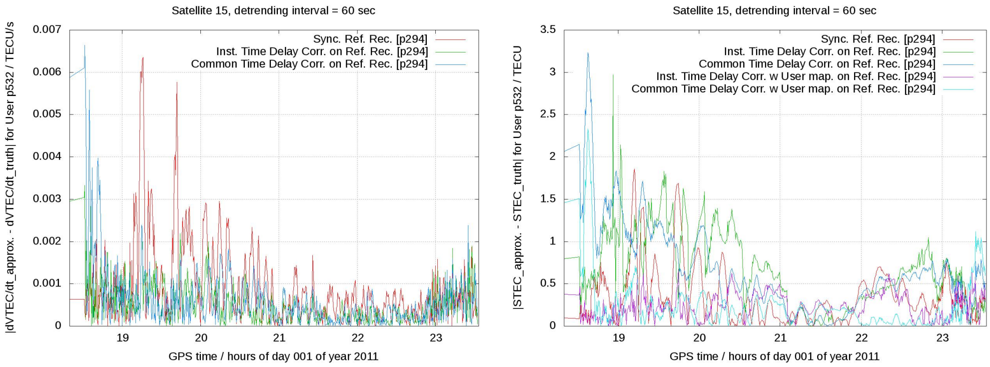

Figure 11. [Left] User VTEC derivative error vs. time, taking as modelled value the zero (red), instantaneous (green) and common (blue) dGII-time-shifted reference site STEC values. [Right] Similar comparison, but for the user STEC, and including as well the VTEC interpolation with the user mapping function for both instantaneous (magenta) and common (light blue) cases (receivers p294 [user] and p532 [ref.], PRN15, day 001, 2011).

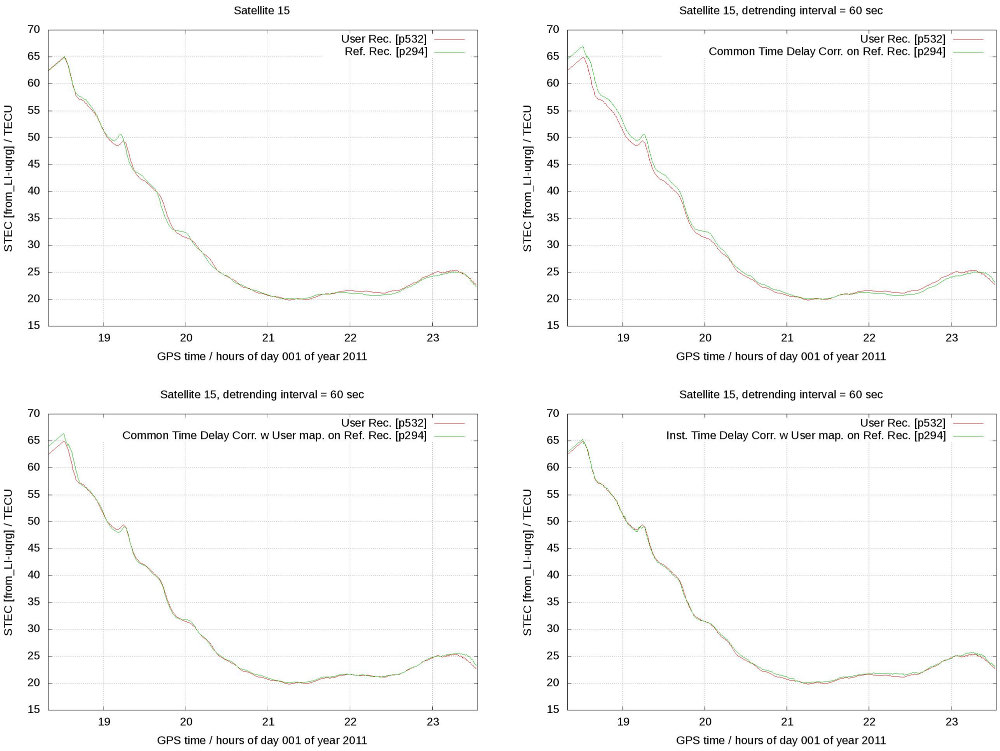

Figure 12. Comparison of original user' STEC with the reference site' STEC: original (LI calibrated with UPC UQRG GIM, top-left), common-time shifted (by the common dGII MSTID time delay, top-right), common-time shifted VTEC + user mapping function (bottom-left) and instantaneous-time shifted VTEC + user mapping function (bottom-right) –receivers p294 [user] and p532 [ref.], PRN15, day 001, 2011-.

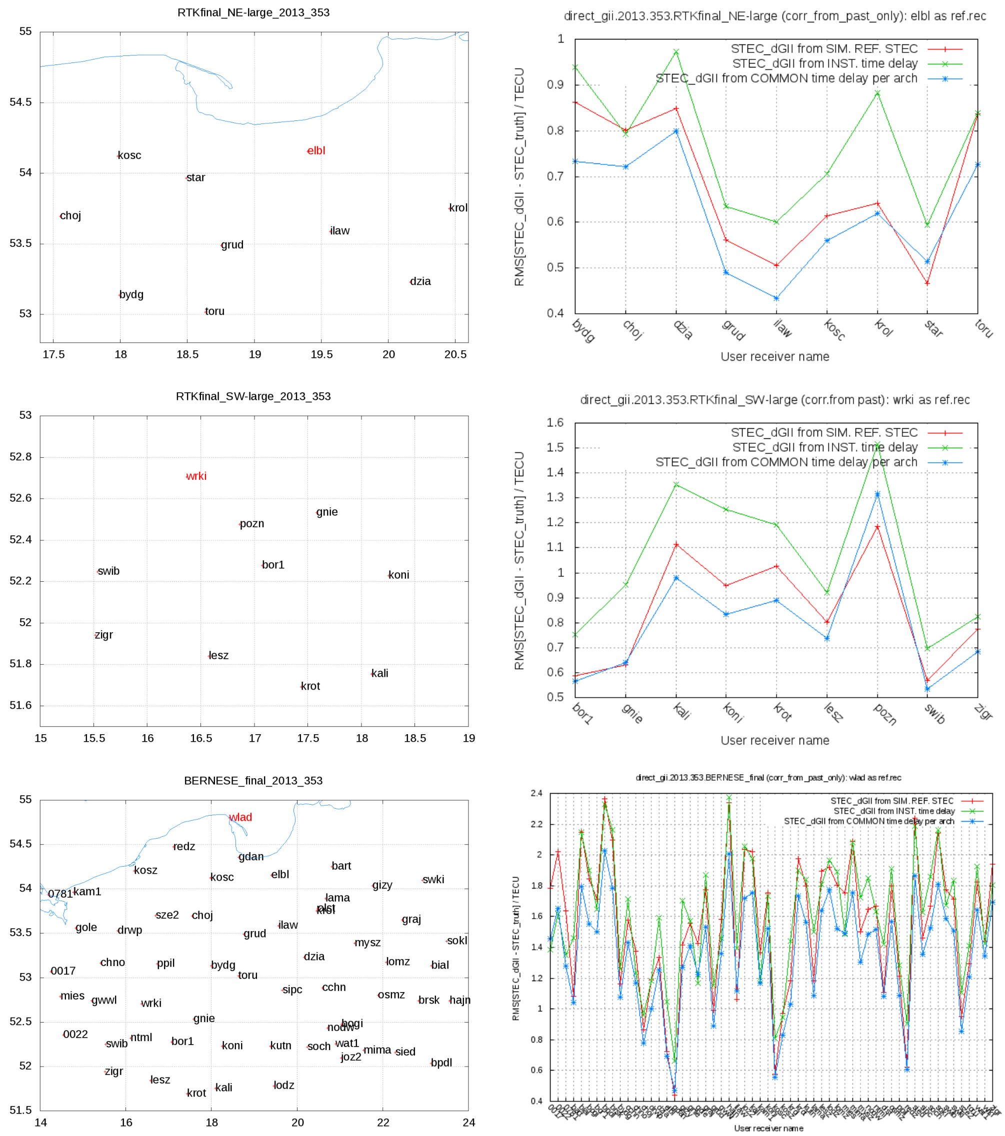

Figure 13. Map of dGII analyzed receivers in RTKfinal-NE-large, RTKfinal-SW-large and BERNESE-final networks (left column), and corresponding performance of dGII for different baselines, with northern reference sites elbl, wrki and wlad, respectively (right column, Poland, winter day of 353, 2013).The performances in the right-hand plots are shown, vs the user receiver name following an alphabetic order, under, i), zero time-shift (red), and time shifts determined by: ii) maximum correlation with the reference receiver ionospheric delay performed instantaneously (green), and, iii), the best value in the continuous arc commonly applied to it (blue).

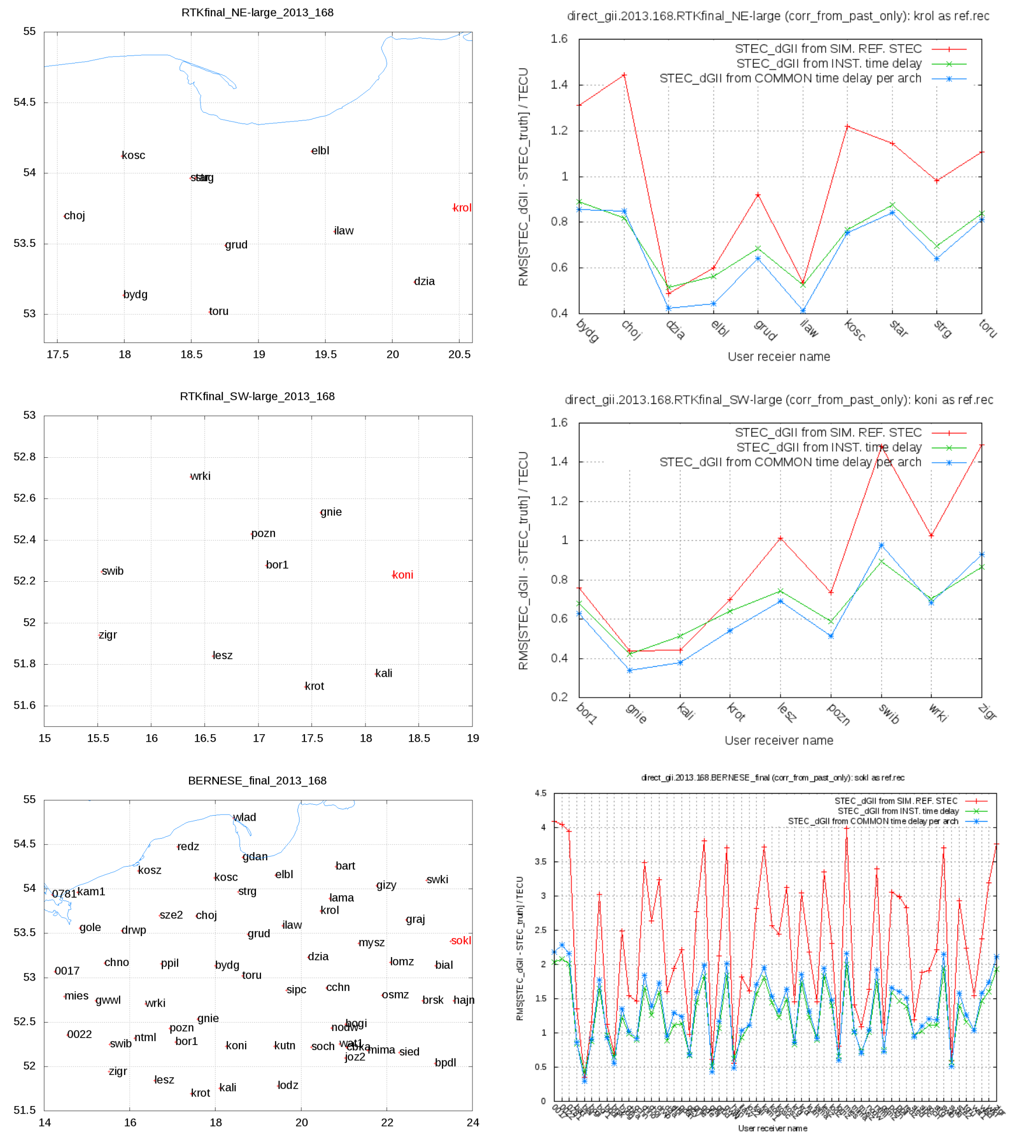

Figure 14. Map of dGII analyzed receivers in RTKfinal-NE-large, RTKfinal-SW-large and BERNESE-final networks (left column), and corresponding performance of dGII for different baselines, with eastern reference sites krol, koni and sokl, respectively (right column, Poland, summer day of 168, 2013). The performances in the right-hand plots are shown similarly to previous figure.

Table 1. Different ionospheric strategies compared on precise GNSS processing

Acronym	Brief description
noSTEC	Observations uncorrected from any ionospheric model
Prop.STEC	Observations corrected with MSTID dGII corrections only
CodeION	Observations corrected with CODE VTEC GIMs
Truth.STEC	Reference STEC values (carrier phase obs. calibrated with UQRG VTEC GIMs)

Table 2. Different type of observation RINEX files considered on precise GNSS processing

Acronym	Brief description
OrgRNX	RINEX file containing original observations
ModRNX	Modified RINEX file containing observations corrected with available ionospheric information
RedRNX	RINEX file with original observations when ionospheric corrections are available only

Table 3. RTK positioning performance statistics, including the standard deviation of the component (std), at central west Poland network on day 168 of year 2013.

Baseline	Strategy	ASR [%]	TTFF [epochs]	N std [m]	E std [m]	U std [m]
BOR1-KONI	RedRNX(noSTEC)	63	29.9	0.011	0.006	0.029
	ModRNX(Prop.STEC)	78	12.8	0.012	0.007	0.035
GNIE-KONI	RedRNX(noSTEC)	74	18.3	0.013	0.008	0.025
	ModRNX(Prop.STEC)	83	15.7	0.013	0.009	0.036

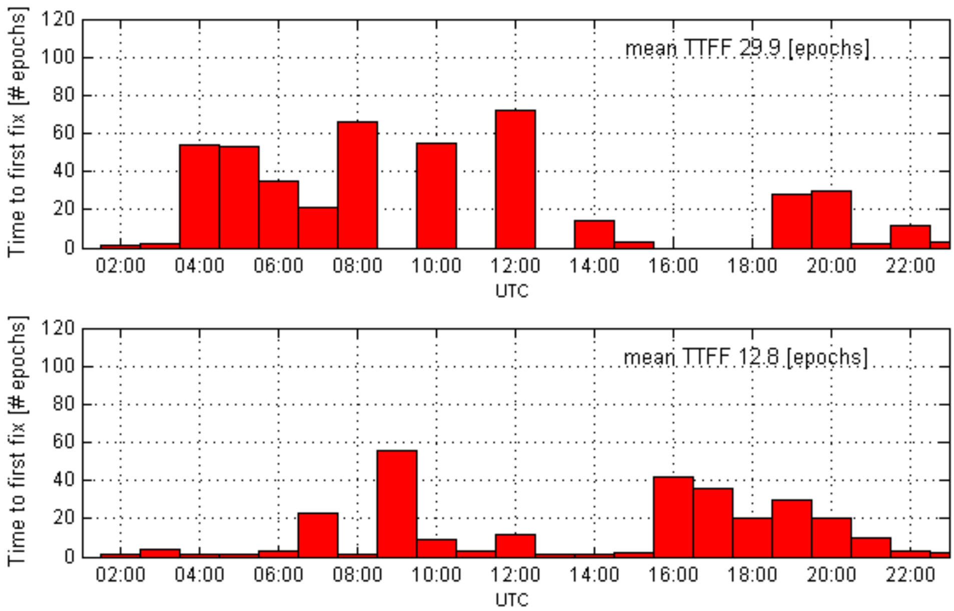

Figure 15. Time To First Fix (TTFF), baseline BOR1-KONI on 168 DOY (top panel- RedRNX(noSTEC), bottom panel- ModRNX(Prop.STEC))

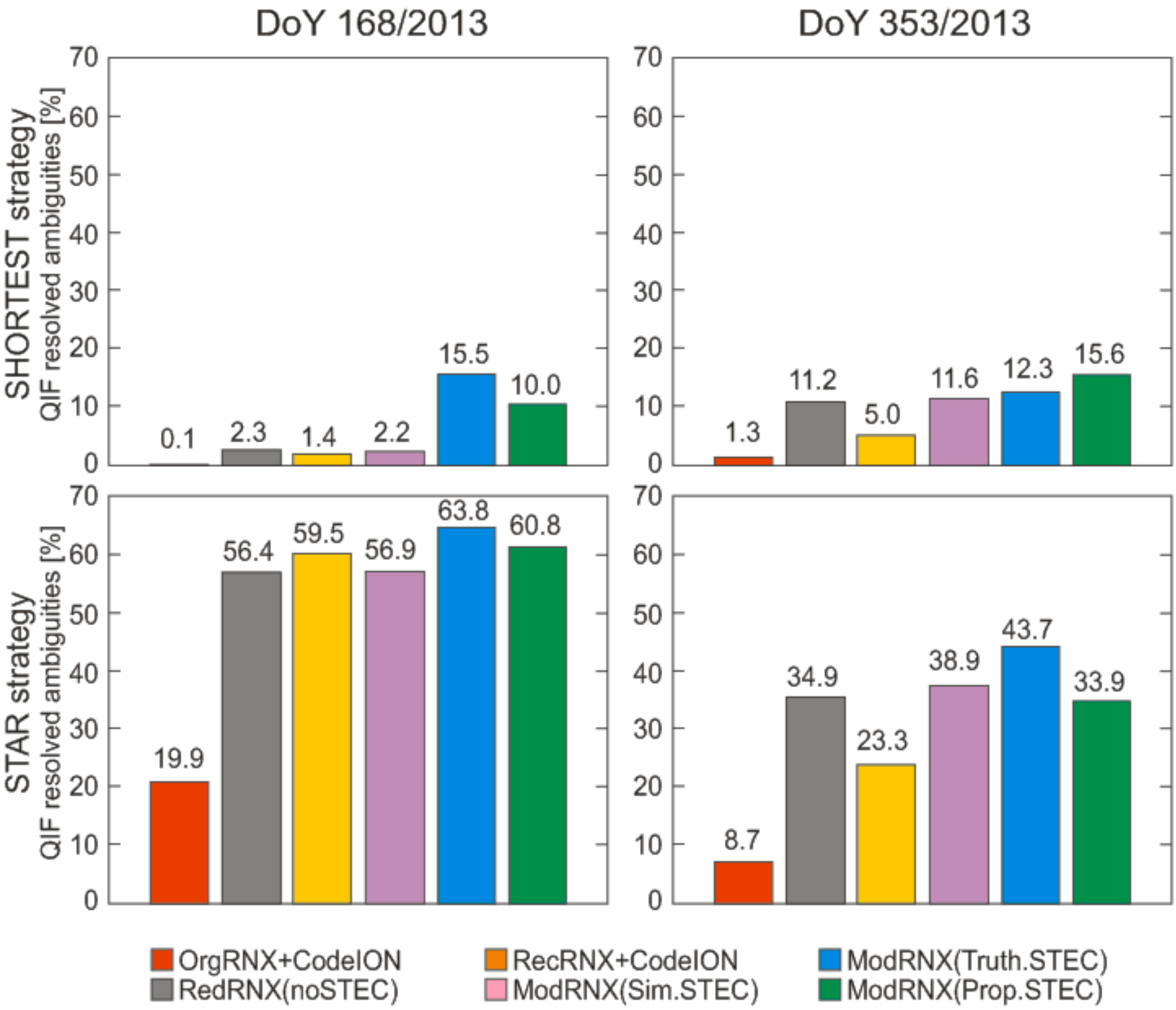

Figure 16. Percent of QIF resolved ambiguities in SHORTEST (top) and STAR (bottom) baseline definition strategies, during summer (left) and winter (right) campaign, for 6 different network solutions.

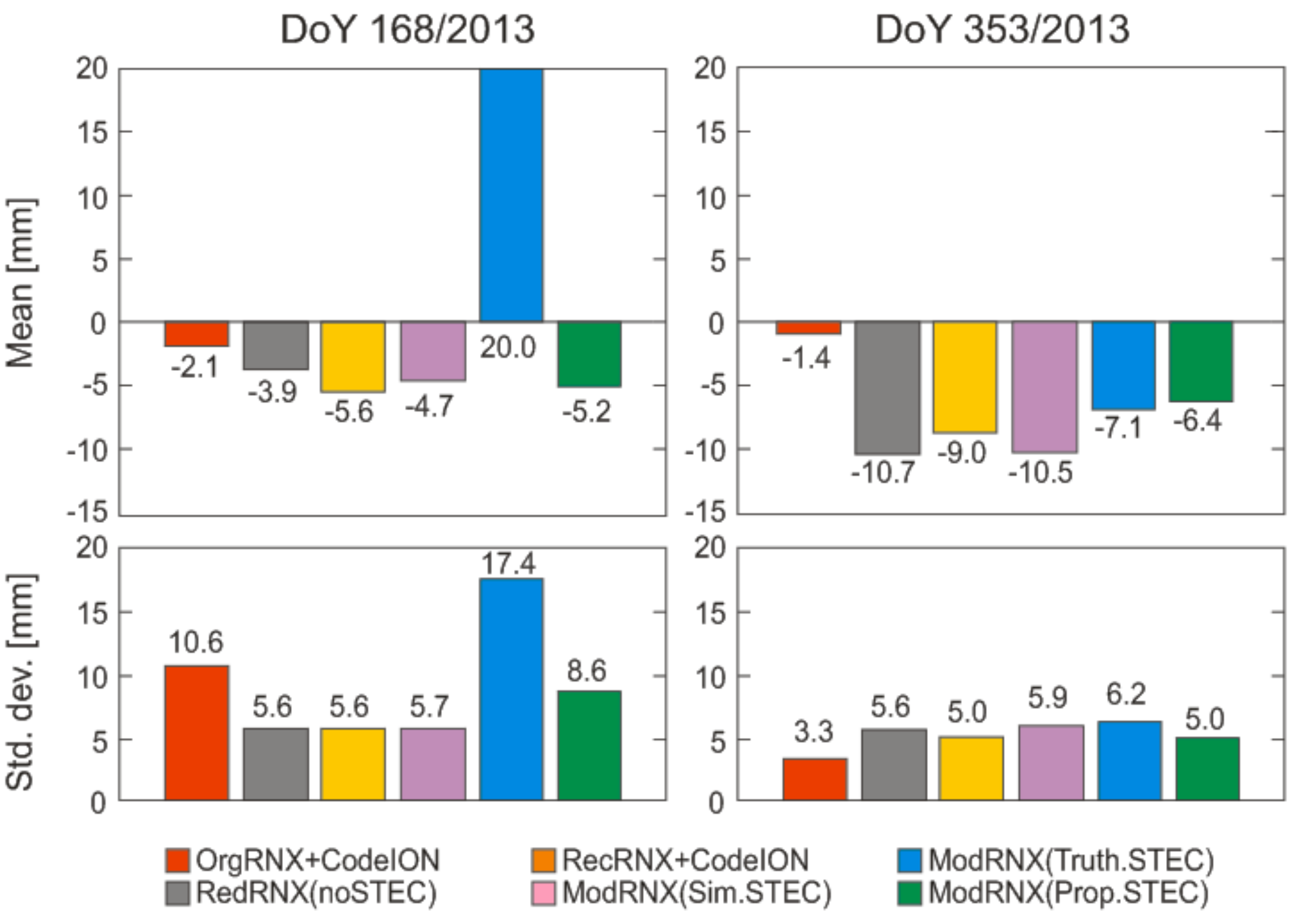

Figure 17. Mean value (top) and standard deviation (bottom) of post-fit residuals between 6 different network solutions with SHORTEST baseline definition and EPN final solution